

Chapter 3

Networking of shear zones at the brittle-viscous transition (Cap de Creus, NE Spain)

Fusseis, F., Handy, M.R. and C. Schrank¹

3.1 Abstract

A crustal-scale shear zone network at the fossil brittle-viscous transition exposed at Cap de Creus, NE Spain evolved by coeval fracturing and viscous, mylonitic overprinting of an existing foliation. Initial fracturing lead to mylonitic shearing as rock softened in ductilely deformed zones surrounding the fractures. Mylonitic shear zones widened by lateral branching of fractures from these shear zones and by synthetic rotation of the existing foliation between the fractures and shear zones. Shear zones lengthened by a combination of fracturing and mylonitic shearing in front of the shear zone tips. Shear zones interconnected along and across their shearing planes, separating rhomb-shaped lozenges of less deformed rock. Lozenges were subsequently incorporated into the mylonitic shear zones by widening in the manner described above. In this way, deformation became homogeneous on the scale of initial fracturing (meter- to decameter-scale). In contrast, the shear zone

¹This chapter was published in the *Journal of Structural Geology* (Fusseis et al., 2006. J. Struct. Geology 28, 1228-1243.)

network represents localization of strain on a decameter-length scale. The strength of the continental crust at the time of coeval fracturing and viscous shearing is inferred to have decreased with time and strain, as fracturing evolved to mylonitic shearing, and as the shear zones coalesced to form a through-going network subparallel to the shearing plane. Crustal strength must therefore be considered as strain- and scale-dependent.

3.2 Introduction

Crustal-scale shear zones are interpreted to transect the lithosphere, extending from the brittle upper crust through the transition to viscous, mylonitic flow in the middle crust down to the viscously deforming lower crust or upper mantle (e.g. Gilbert et al., 1994, Thatcher & England, 1998). Exhumed, ancient segments of this transition, here termed the brittle-viscous transition (BVT), usually consist of a system of networked shear zones (Mitra, 1979, Choukroune & Gapais, 1983, Hobbs et al., 1986, Gapais et al., 1987) in which brittle and viscous deformation are mutually overprinting (e.g. Passchier, 1984, Hobbs et al., 1986).

Knowledge of the temporal and kinematic evolution of shear zone networks at the BVT is crucial for understanding the evolution of crustal rheology at the BVT. Due to the broadly coeval activity of brittle and viscous deformation mechanisms, this rheology is expected to be sensitive to several parameters, primarily effective pressure, temperature and strain rate (e.g. Sibson, 1980, Hobbs et al., 1986, Handy et al., in press).

Shear zone networks (SZNs) have been studied in nature (e.g. Mitra, 1979, Bell, 1981, Choukroune & Gapais, 1983, Gapais et al., 1987, Lafrance et al., 1998, Stewart et al., 2000, Carreras, 2001, Imber et al., 2001, Arbaret & Burg, 2003), as well as in experiments (e.g. Cobbold et al., 1971, Harris & Cobbold, 1985, Dennis & Secor, 1987, Williams & Price, 1990, Herwegh & Handy, 1996, Huddleston, 1999), with most work devoted to the kinematics of strain partitioning in a system of networked shear zones. Other contributions deal with theoretical aspects of rheology as well as the dynamics of SZNs (Handy, 1994, Regenauer-Lieb & Yuen, 2003), but little is known about how shear zones actually network (Arbaret & Burg, 2003).

The mylonite belt at the Cap de Creus, northeastern Spain (Fig. 3.1a), allows insight into the evolution of a crustal-scale shear zone network that

formed in quartz-rich metasedimentary rocks under greenschist-facies conditions at the BVT. Available age constraints indicate that the mylonite belt probably formed during the late stages of the Variscan orogeny (Druguet, 2001). Carreras (2001) proposed nucleation models that apply to most of the large-scale folds, shear zones and shear zone networks in the Cap de Creus mylonite belt. In this paper, we present a complementary model for the evolution of those parts of the Cap de Creus mylonite belt where the close spatial and temporal association of brittle fracturing and viscous, mylonitic shearing cannot be explained by these previously published models.

It will be shown that shear zones originated as shear fractures before coalescing to form a network of mylonitic shear zones. Once networked, the shear zones widened by a combination of fracturing and mylonitic shearing. Initially heterogeneous and highly localized strain was transformed into a system of decameter-wide shear zones. Deformation became homogenized on the initial scale of fracturing, while becoming heterogeneous on a larger length scale. Specialized structural terms used in the text are defined in Appendix 9.1 and are printed in italics where they appear in the text for the first time.

3.3 Geological setting

The protolith rocks of the shear belt at the Cap de Creus peninsula are late Precambrian or Cambro-Ordovician age metasediments (Druguet & Hutton, 1998) consisting of mostly psammitic and pelitic layers. During the Variscan orogeny, these sediments experienced a low-pressure, greenschist- to amphibolite-facies metamorphism which increases in grade from SW to NE on a much longer length scale than the investigated shear zones (Fig. 3.1b, Druguet, 2001). At least three deformational events can be discerned during this metamorphism:

1. S1 developed parallel to bedding, S0, prior to the peak of metamorphism, yielding a composite foliation, S0/1. This D1 deformation involved boudinage and isoclinal F1 folding of quartz segregations.
2. During D2 the composite S0/1 was folded and sheared under peak, amphibolite-facies conditions, leading to the formation of a composite S1/2 in the E-W trending limbs of tight to isoclinal F2 folds (e.g.

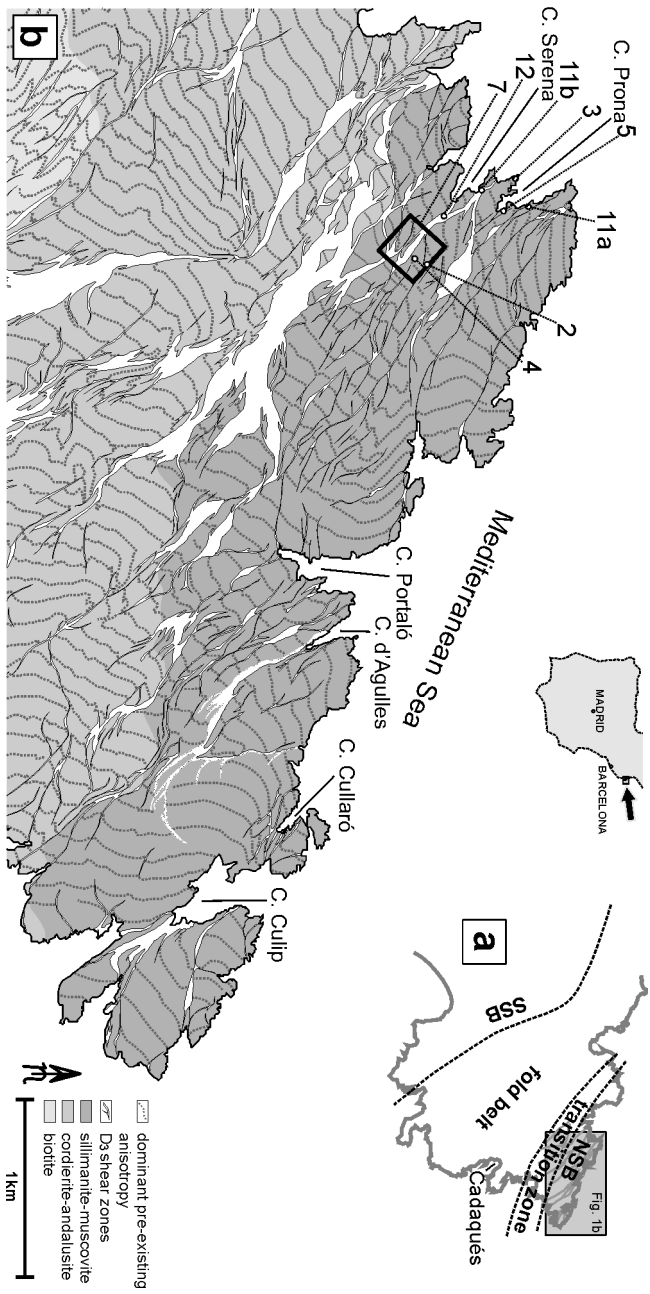


Figure 3.1: Close-up of the northern Cap de Creus peninsula: (a) Schematic map of the deformation at the Cap de Creus. SSB - Southern Shear Belt, NSB - Northern Shear Belt, from Carreras (2001); (b) Structural map of the northern Cap de Creus peninsula showing the metamorphic zonation, the principal trends of the dominant S1/2 foliation (dotted line is a composite of S0/1 and S1/2) and the D3 shear zones forming the "Northern Shear Belt" (in white). Insets mark the locations of figures below. Modified from Carreras (2001) and Druguet (2001).

in the Cala Serena and Cala Prona areas in Fig. 3.1, see also Carreras et al., 2005). The amplitudes of these folds vary from centimeter to meter scales depending on the initial thickness of the sedimentary layers. Fold limbs are strongly thinned (Fig. 3.2). The D2 shear plane was oriented ESE-WNW and shearing on the km-scale involved dextral, non-coaxial flow (Druguet et al., 1997, Bons et al., 2004). Locally, melt-bearing layers developed synchronously with S2 (Druguet & Hutton, 1998), whereas granitoids and pegmatites intruded prior to or during D2 (Druguet, 2001, Bons et al., 2004).

3. D3 deformation is marked by several structural domains in the northern part of the Cap de Creus peninsula (Fig. 3.1), described here in order of increasing strain intensity: In the southwest, open to close F3 folds without shear zones ("fold belt" in Fig. 3.1a) are gradational to the northeast to a domain of asymmetrical F3 folding (cf. fig. 12 in Carreras, 2001). Further to the NE, these folds have sheared limbs and fold axes parallel to L3 stretching lineations (defined by aligned quartz and feldspar), and are transitional to retrograde, greenschist-facies shear zones that crosscut all pre-existing fabrics ("transition zone" of Carreras, 2001, Carreras & Casas, 1987). In the northeasternmost part of the Cap de Creus peninsula, these shear zones become interconnected to form the "Northern Shear Belt" (Carreras & Casas, 1987). Their kinematics reflect right-lateral transpressive shearing (Carreras, 2001).

In the northernmost Cap de Creus, D3 began at around 560°C and 2.4 Kbar (Druguet, 2001), conditions that are corroborated by the dynamic recrystallization of feldspars in pegmatite (e.g. Tullis & Yund, 1991). Quartz in D3 mylonites recrystallized by subgrain rotation and grain boundary bulging, indicating syndeformational temperatures of $450\pm 50^\circ\text{C}$ at geologically reasonable strain rates (Stipp et al., 2002, Füsseis & Handy, 2006). No signs of static recrystallization were found in D3 mylonites. D3 was therefore active in a temperature interval corresponding to upper- to sub-greenschist facies conditions.

Our investigation focussed on selected parts of the "Northern Shear Belt". This shear belt typically consists of two sets of shear zones (Fig. 3.1b): (1) NW-SE trending, shallowly NE-dipping shear zones that accommodated top-SE shear parallel to moderately NW-plunging stretching lineations; (2)

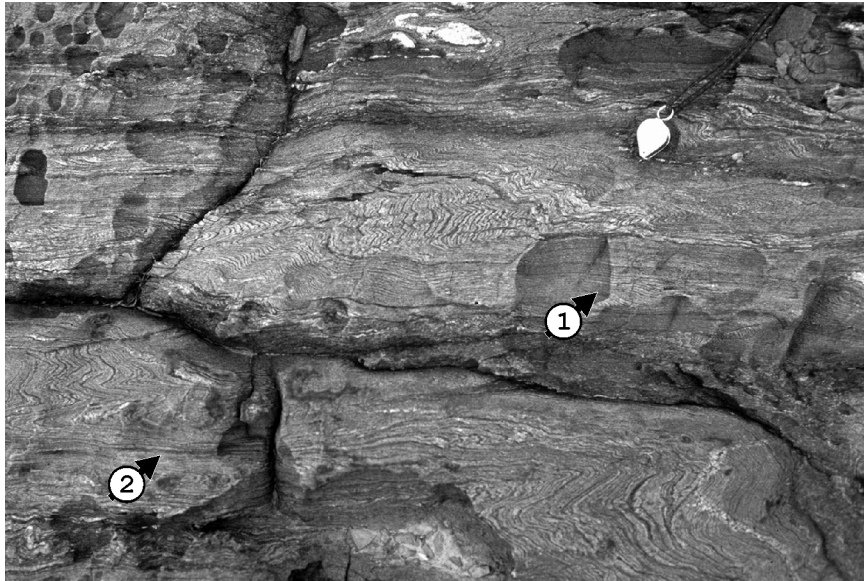


Figure 3.2: Photograph of D2 folds and associated S1/2 composite foliation in the host rock for the D3 shear zones. Note the thinned layers of S0/1 in the sheared fold limbs forming S1/2 (arrows 1 and 2). D2 folding generally varies in intensity. Folds may be more symmetric than shown in this picture (see foliation trajectories in Fig. 5). Photograph was taken looking towards the N, hand lens for scale. UTM 31T 522017 east, 4686974 north.

interlinking E-W trending, northward-dipping shear zones with more steeply NW-plunging stretching lineations. The latter either accommodated oblique thrusting towards the SE or oblique-slip, down-dip movement towards the NW. As shown below, these movements all occurred within a common kinematic framework and the observations described below indicate that differently oriented shear zones interacted to accommodate deformation compatibly on the kilometric scale of the entire shear belt.

3.4 Nucleation and growth of shear zone networks at the BVT

The nucleation, growth and networking of shear zones are best exposed in the Cala Serena and Cala Prona areas, along the northern shore of the Cap de Creus peninsula (Fig. 3.1b). By tracing these shear zones across and along their strike, we were able to establish a preserved sequence of three evolution-

ary stages. This space-for-time substitution is based on the premise that all the shear zones developed during one continuous tectonometamorphic phase (D3), an assumption that is supported by our observations described below.

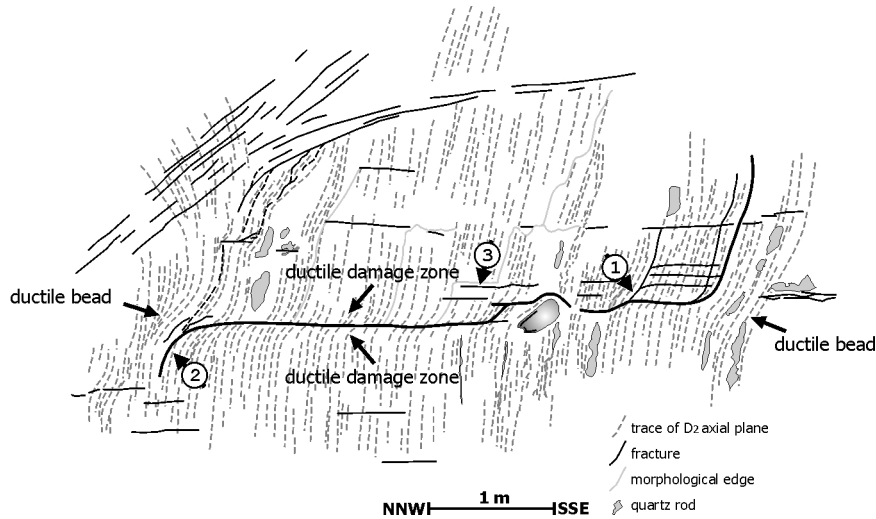


Figure 3.3: Sketch map of a shear fracture at the northernmost tip of the peninsula separating Cala Serena from Cala Prona. Note bending of S1/2 marking the ductile bead, as well as the fault drag along the fracture. See text for explanation. UTM 31T 521586 east, 4687501 north.

3.4.1 Strain localization within fractures

Over the entire area, mylonitic shear zones are associated with fractures that occur either individually parallel to the overall D3 shear plane (trending NW-SE and dipping to the NE, Figs. 3.3, 3.4) or emerge from the tips and margins of mylonitic shear zones (arrows 4 to 6 in Figs. 3.5a, Fig. 3.11). Both kinds of fracture never crosscut D3 mylonites and displacement along them is consistent with the overall dextral shear sense of the D3 shear zones (Figs. 3.3, 3.4).

Individual fractures range in length from a few centimeters to about three meters. Longer fractures up to 10m long consist of several interconnected fracture segments (Figs. 3.3, 3.4). Where no mylonitic shear zones formed, the rock contains fractures up to several meters in length with no slip and no signs of a *ductile damage zone* around them.

Faults show warped S1/2 surfaces that form a monocline beyond their tips. These monoclines correspond to the "ductile beads" described by Elliott (1976, arrows in Figs. 3.3, 3.4). The S1/2 surfaces along the faults show a *normal drag*, with *sharp cut-offs* where they intersect the fracture plane. The normal sense of drag is consistent with the movement inferred from monoclinical folding of S1/2 in the ductile bead (arrows in Figs. 3.3, 3.4).

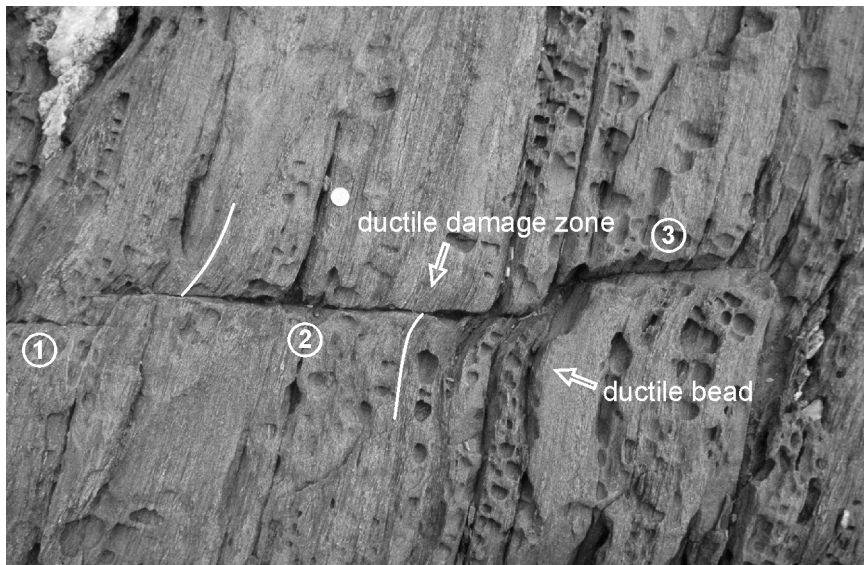


Figure 3.4: Three, longitudinally linked shear fractures (labelled 1, 2, 3) on the eastern slope of southern Cala Serena. Note the flexure of S1/2 forming a ductile bead beyond the fracture tips and the drags with the sharp cut-offs along the central fracture (white lines). Note that white lines illustrate dragging of S1/2 and do not denote a marker. Photograph is taken looking towards the E, diameter of coin is 2,3cm. UTM 31T 521959 east, 4686946 north.

Fault tips often splay anticlockwise from the shearing plane to become parallel to S1/2 away from the fractures (arrows 1 and 2 in Fig. 3.3). These splays are more pronounced in metapsammites than in metapelites. Modes of fracturing and sense of shear along these tip fracture segments could not be determined macroscopically. In few cases, fault tips curve clockwise into a high-angle orientation with respect to S1/2. Anticlockwise splays probably reflect the influence of S1/2 (Ivins et al., 1990, Ranalli & Yin, 1990, Yin & Ranalli, 1992) as well as of changed principal stress orientations at fault tips (e.g. Vermilye & Scholz, 1999) on propagating fractures. In contrast, clockwise curving fault tips resemble fault terminations in homogeneous rocks

(horse-tail splays, e.g. Kim et al., 2004).

Existing lithological variations (a $100\mu\text{m}$ - 2mm spaced foliation on the microscopic scale and a 20-200cm thick layering on the outcrop scale, Fig. 3.5b) influence fracture propagation. On the microscopic scale, fractures are usually deflected by mica-rich S1/2 cleavage domains, where they tend to form shear bands, whereas Qtz- and Fsp-dominated microlithons are cross-cut obliquely by narrow fractures (Fusseis & Handy, 2006). On the outcrop scale, faults and also mylonitic shear zones that crosscut metapelitic layers show relatively narrow drags. Besides these, however, no systematic variations of style, orientation or spacing were found that might have been caused by the different lithologic variations.

3.4.2 Shear zone nucleation and propagation

Fig. 3.5 shows the termination of a shear zone within metagreywackes and metapelites. The displacement of markers decreases continuously from the middle of the shear zone at the left to the tip at the right (Fig. 3.6). Based on the evaluation of displacements along single faults (eg. Cowie & Scholz, 1992a, Cowie & Shipton, 1998) as well as on microstructural observations (Fusseis & Handy, 2006), we interpret this relationship to show that the tip of the shear zone developed most recently, whereas the middle of the shear zone was active longer. Therefore, a succession of deformation increments can be studied from tip to middle along the length of the shear zone.

The actual shear zone termination consists of parallel shear fractures, typically between 50 and 150cm, long that accommodate a fraction of the total displacement and cross-cut slightly refolded D2 axial planes (arrow 1 in Fig. 3.5a). The fractures overlap and separate intervening volumes of less-deformed rock. S1/2 sometimes appears to have rotated synthetically in these intervening domains. Microstructural investigations reveal that fractures contain narrow seams of fault rock consisting of aligned biotite, quartz and feldspar (Fusseis & Handy, 2006). Towards the left in Fig. 3.5, S1/2 is increasingly dragged and becomes almost parallel to the D3 shearing plane in its most strongly deflected, central part (arrow 2 in Fig. 3.5a). In this part of the shear zone, fractures are more closely spaced and segment the D2 fabric. The total displacement in this domain is distributed among slip on closely-spaced shear fractures, on the deflected S1/2, as well as on rotated S1/2 between the fractures.

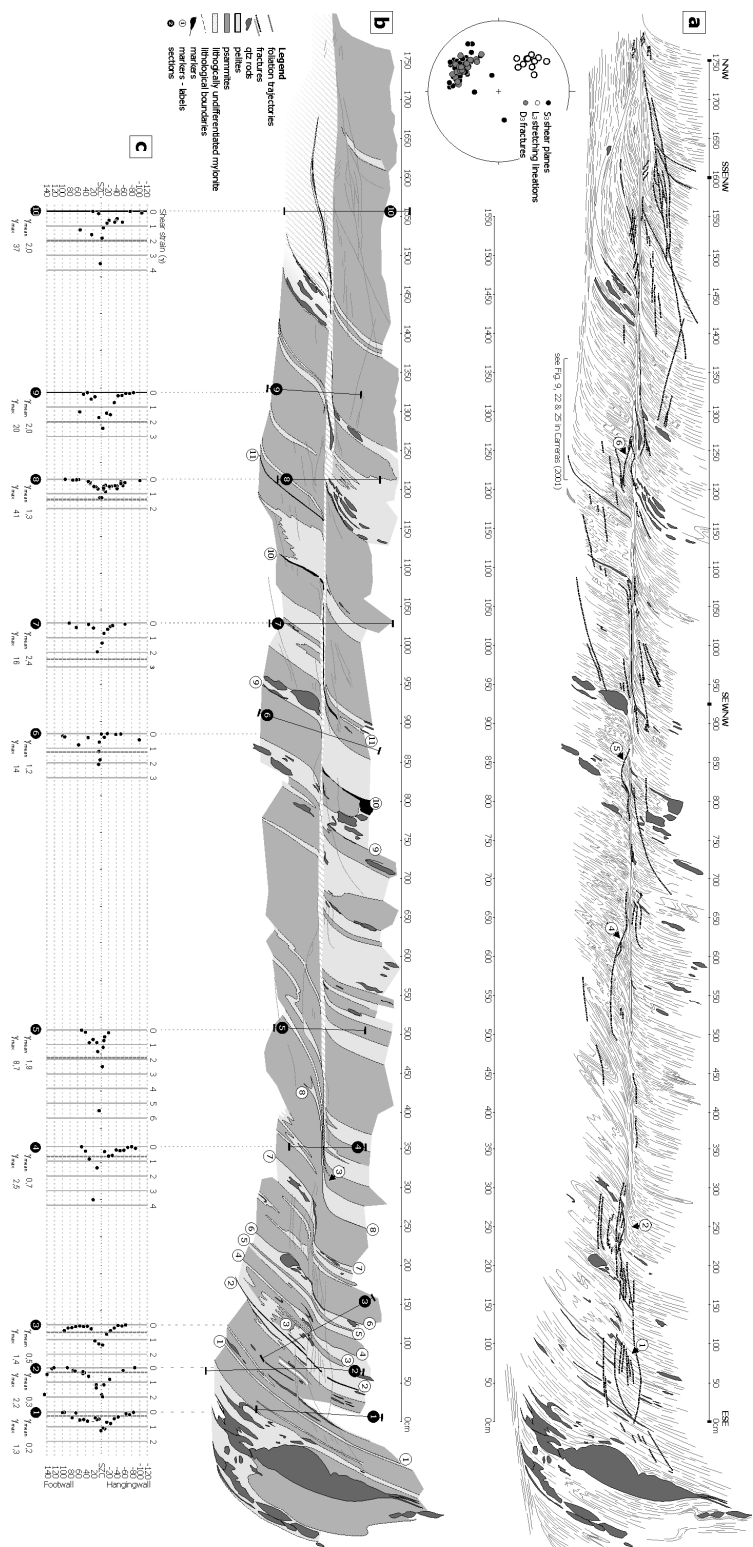


Figure 3.5: Shear zone termination in the Cala Prona (cf. fig. 21 in Carreras, 2001): (a) Sketch map shows foliation trajectories, fractures and deformed quartz rods along the shear zone. Inset equal area projection shows S3, fractures and stretching lineations L3 measured along the shear zone; (b) Map illustrates the sheared lithologies and individual markers used for measuring the displacement. Also shown are the positions of investigated sections across the shear zone; (c) γ vs. Wsect plots calculated for the sections in (b); SZC - shear zone centre. UTM 31T 521767 east, 4687430 north.

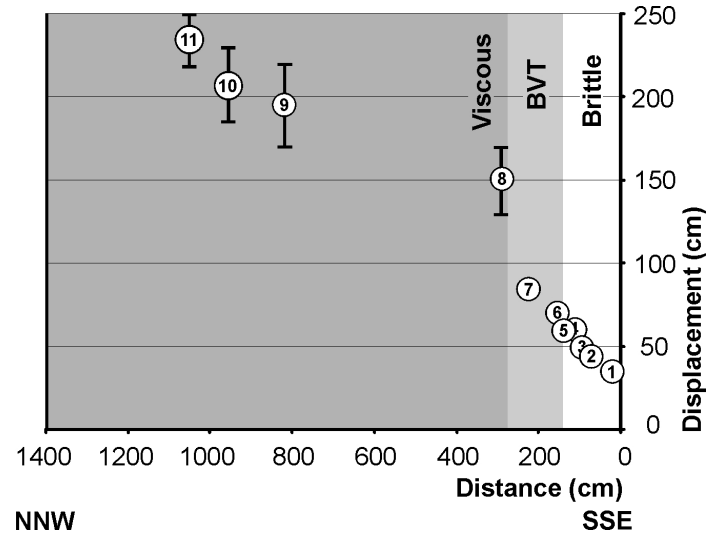


Figure 3.6: Displacement vs. distance plot for the markers labelled in Fig. 3.5b. Note the continuous increase in displacement with increasing distance from the fault tip, especially across the transition from predominantly brittle fracturing to mylonitic shearing. The error bars represent broad and conservative estimates of the displacements that result from uncertainties due to the uneven outcrop morphology.

The relatively oldest, central part of the shear zone consists of smooth marginal drags and a mylonitic center approximately 15cm wide where most of the displacement is accommodated and no fractures occur. D2 fabrics in ductile drags are gradually mylonitically overprinted towards the shear zone center (Carreras & García-Celma, 1982, Garcia-Celma, 1983). Significant grain-size reduction is observed. Layers of folded S0/1 rotate into parallelism with the D3 shearing plane and are significantly thinned (arrow 3 in Fig. 3.5b). Nevertheless, individual markers (quartz rods and lithological beds) can be traced across the shear zone (Fig. 3.5b).

We quantified the strain evolution in ten sections across the shear zone by measuring S1/2 orientations and applying Ramsay & Graham's (1970) method of calculating the shear strain (γ) distribution (App. 9.2). Slip on S1/2 itself could not be quantified and thus was not considered in these calculations. Therefore, the calculated γ -values may be slight underestimates of the actual shear strain.

Curved drags indicate that γ is not distributed homogeneously across the shear zone (Ramsay & Graham, 1970). The maximum shear strain in the shear zone center (γ_{max}) was estimated using a procedure described in

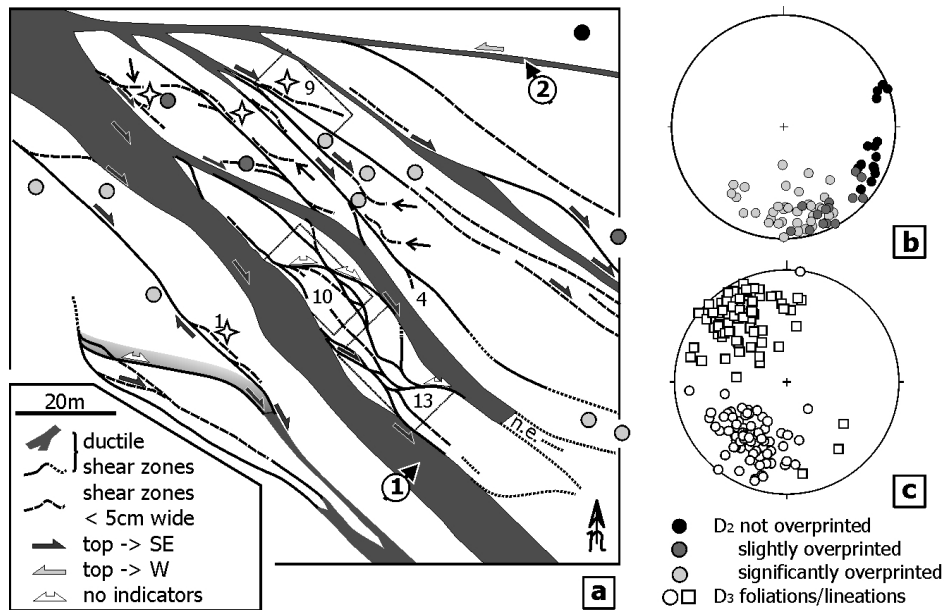


Figure 3.7: Shear zone network in the SE part of the Cala Serena valley, where different stages of shear zone networking can be observed: (a) Map of SZN. Inset boxes correspond to Figs. 3.9, 3.10 and 3.13. Label "4" marks the position of Fig. 3.4. Grey shaded and black circles correspond to sites where the orientation of S1/2 was measured. Note that the intensity of shading corresponds to the qualitatively estimated intensity of D3 overprint (black - not overprinted, light grey - significantly overprinted). White stars indicate outcrops where drag truncation can be observed. n.e. - not exposed; (b) Equal area projection shows orientation of S1/2 outside the SZN and in lozenges. See bottom right corner for colour codes. Dataset = 69 measurements; (c) Equal area projection illustrating poles to D3 shear zones (circles) and associated stretching lineations (squares). Dataset = 75 measurements. Database for slip line analysis in Fig. 3.8.

Appendix 9.2. The average shear strain (γ_{mean}) was calculated by dividing the total displacement across a particular section by the local shear zone width, W_{sect} at that section (data listed in Table 3.1).

Both γ_{mean} and γ_{max} increase along the shear zone from SE to NW, from the shear zone termination to the mature segments. Due to the almost constant width of the shear zone, γ_{mean} increases almost linearly with displacement, from 0.2 at section 1 to 2.0 at section 10 in Figure 3.5c. γ_{max} increases non-linearly from 1.28 at section 1 to > 37 at section 10, especially towards the left of section 4 (see Figs. 3.5b&c) where all displacement is accommodated within the center of the mylonitic shear zone. We interpret this to indicate that strain softening occurred in the shear zone center relative

to the propagating tip.

Lateral terminations of meter- to decameter-long shear zones could not be mapped in the investigation area. However, we propose that these terminations look similar to the described leading and trailing terminations, since the mechanisms by which the rock deforms are the same. The varied orientation of S1/2 with respect to the lateral shear zone terminations is a factor that may influence the geometry of the resulting tip process zone. However, the ductile beads that have been described from mode III terminations of thrust faults (Elliott, 1976) resemble the ones shown in this paper (Figs. 3.3, 3.4, 53.5).

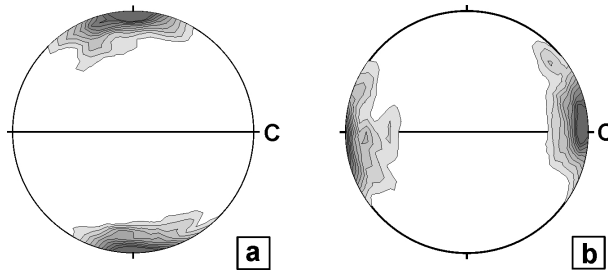


Figure 3.8: Slip line analysis (method of Gapais and Cobbold, 1987, Gapais et al., 1987) of the southern Cala Serena SZN: (a) Poles to D3 shear zones; (b) L3 stretching lineations. "C" indicates inferred macroscopic shearing plane oriented E-W for reference. Dataset 75, contours at 1, 2, 3, 4, 5, 6, 7, 8, 9, 10% of a uniform distribution. See text for explanations.

3.4.3 Shear zone interconnection and strain homogenization

Shear zones that exceed several meters in length are interconnected with neighboring shear zones to form three-dimensional networks. These shear zone networks comprise interconnected, NW-SE trending host shear zones and E-W trending step-over shear zones, as observed in the southern Cala Serena (Fig. 3.7a). The most prominent host shear zone trends NW-SE through the center of the mapped area (arrow 1 in Fig. 3.7a). It is connected to a sinistral step-over shear zone trending E-W (arrow 2 in Fig. 3.7a). Between the two, NW-SE trending, decimeter- to meter-wide mylonitic host shear zones splay at a roughly regular 10-20m distance from the sinistral shear zone (Fig. 3.7a). Most of these subordinate host shear zones have brittle terminations in the SE, which indicates that these narrower host shear zones nucleated along the sinistral master fault and propagated towards the

SE. The host shear zones are interconnected by several step-over shear zones. The lateral distance between the host shear zones is about half the along-strike distance between the step-overs. This initial network of host and step-over shear zones defines rhomb-shaped lozenges of less deformed rock with lengths between 15 and 30m and widths of 5 to 10m (Fig. 3.7a). S1/2 in these lozenges is reoriented with respect to the undeformed domains outside the network (Fig. 3.7b). The orientations of all mylonitic shear zones and shear fractures are plotted in Figure 3.7c.

Figure 3.8 shows the poles to the D3 shear zones and associated L3 stretching lineations with respect to the overall shearing plane, C3. C3 is depicted in a horizontal E-W orientation for reference (horizontal equator in Fig. 3.8). The asymmetry of the S3 foliation poles with respect to C3 is partly caused by step-over shear zones that emerge from host shear zones and connect them at an acute angle to the overall shear plane (Fig. 3.7). The overall pattern of S3 and L3 in Figure 3.8 is diagnostic of a strong component of simple shearing during D3 (Gapais et al., 1987, see below).

Most step-overs are parallel to S1/2 (Fig. 3.9, small black arrows in Fig. 3.7) or cut S1/2 at acute angles. Step-overs can be found in different evolutionary stages, from precursory brittle fractures without visible slip and without macroscopically visible fault rock (arrows in Fig. 3.7a), to narrow shear zones containing a black and very homogeneous, ultra-mylonitic fault rock (Fig. 3.9), to wider ductile shear zones with fine-grained, homogeneous mylonitic fabrics (Fig. 3.10). Similar to the host shear zones, we interpret this sequence of stages to represent a continuous evolution with increasing displacement. Unambiguous shear-sense indicators are rare in step-over shear zones, irrespective of scale. If shear sense indicators are found, then in roughly equal numbers of opposing indicators (Fig. 3.7a). We interpret this to indicate a complex deformation history (see discussion).

Some shear zones are wider and the lozenges between them are smaller (Figs. 3.12, 3.13). We interpret wider shear zones to have accommodated more displacement than narrower ones. Shear-zone widening involves slip on and propagation of fractures cross-cutting the dragged foliation in the rock next to mylonitic shear zones in a process termed drag truncation (Figs. 3.11a, b). Fractures truncating drags can be found in the foot- as well in the hanging wall of mylonitic shear zones (Fig. 3.5, arrows 4 to 6, Fig. 3.11b, arrow 4). In some cases, these fractures link at their rear (NNW-most extent)

Section (NW <> SE)	10	9	8	7	6	5	4	3	2	1
Distance from SZ-tip (cm)	1570	1325	1220	1030	880	500	350	120	70	10
D_{sect} (cm)	324	279	261	225	200	131	104	60	45	30
W_{sect} (cm)	160	140	198	95	170	70	140	120	160	185
HW drag (from-to, cm)	-106 to -3	-55 to -5	-105 to -2	-32 to -9	-118 to -2	-50 to -8	-50 to -10	-55 to -65	-72 to 88	
HW damage zone displacement (cm)	52	21	39	13	39	17	31	56	102	40
FW drag (from-to, cm)	2 to 54	5 to 85	3 to 93	3 to 63	9 to 52	4 to 20	10 to 90	-	-	-
FW damage zone displacement (cm)	88	56	19	18	4	10	22	-	-	-
SZ Centre (from-to, cm)	-3 to 2	-5 to 5	-2 to 3	-9 to 3	-2 to 9	-8 to 4	-10 to 10	-	-	-
γ_{max}	37	20	41	16	14	8,7	2,5	1,37	2,23	1,28
γ_{mean}	2,0	2,0	1,3	2,4	1,2	1,9	0,7	0,5	0,3	0,2

Table 3.1: Structural data from Sections 1 to 10 across the shear zone in Fig. 3.5b. The dataset documents a gradual increase in displacement from SE to NW, as well as increasing divergence between γ_{max} and γ_{mean} . The shear zone width W_{sect} is approximately constant. Displacements were interpolated from the data plotted in Fig. 3.6. See App. 9.1 for terminology.

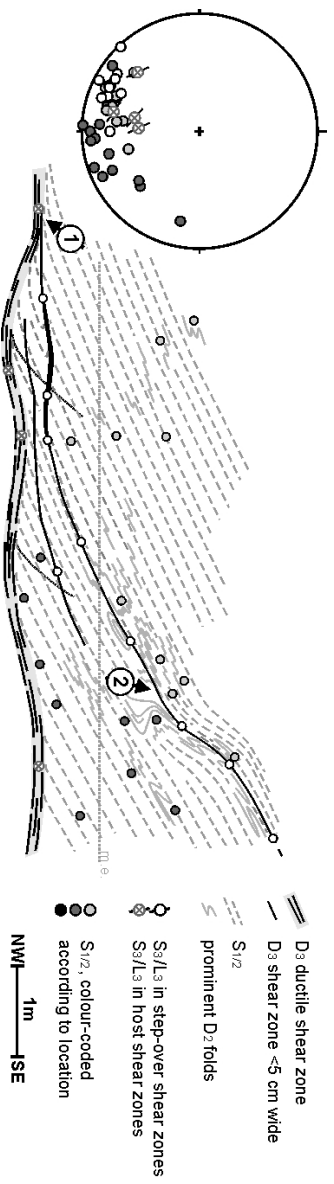


Figure 3.9: Sketch map showing a step-over shear zone containing thin black ultramylonite that branches from a host shear zone at the left margin of the picture (arrow 1). The step-over shear zone follows S_{1/2} (arrow 2). The equal area plot illustrates that the orientation of S_{1/2} varies in the foot- and hanging walls of the step-over shear zone. The step-over itself is parallel to the hangingwall fabrics. Note the shading of different fabric domains. S₃/L₃ orientations for mylonitic shear zones are plotted with the method of Hoepfner (1955). 'm.e.' indicates a morphological edge of the outcrop. Legend applies to Figs. 3.10 and 3.13. UTM 31T 521933 east 4686984 north.

with other fractures emerging from the mylonitic shear zone center (arrow 1 in Fig. 3.11a), whereas in other cases they propagate towards the shear zones centers themselves (arrow 5 in Fig. 3.11b). The rock between the fracture and the shear zone center is decoupled from the host rock (arrow 2 and shaded area in Fig. 3.11a, stars in Fig. 3.7). Fabrics within the isolated domains are usually reoriented with respect to the foliation outside. This reorientation involves a component of flexural slip parallel to $S1/2$ (Carreras & Garcia-Celma, 1982, Garcia-Celma, 1983).

Fractures which segment the drag are interpreted to have existed either prior to the onset of mylonitic shearing (e.g. arrow 3 in Fig. 3.3) or to have formed during dragging and mylonitic shearing. An example of drag truncation in Figure 3.11 shows a successive reorientation of the wall-rock foliation from the fault's propagating tip (right) towards its rear (left, Fig. 3.11a, inset equal area plot). The decoupled fabric experiences pronounced (D3) mylonitic overprint during rotation. Reorientation and mylonitic overprint increase in intensity from left (NNW) to right (SSE, see equal area plot in Fig. 3.11a). The rock at the left (rear) end of the truncated drag is macroscopically indistinguishable from the mylonite in the shear zone center below. The subsidiary fault drag which evolves along the NW end of the fracture and its termination as a mode 1 fracture at the SE end indicate that the fracture propagated towards the right (SE).

Truncated drags are between 0.1 and 1m wide and 0.2 to 8m long (Figs. 3.7a, 3.11). There seems to be a relation between the scale of the truncated drags and the width of the involved shear zones which could not be quantified yet. En-echelon arrays of truncated drags were observed in the Cala Serena (star 1 in Fig. 3.7a). Drag truncation occurs along step-over shear zones as well as along host shear zones, and thus compartmentalizes lozenge interiors. Once the tips of fractures truncating the drags connect with other shear zones, the resulting compartments form smaller-scale lozenges. Figure 3.10 shows a step-over that separates two lozenges. Towards its right and below its junction with the upper host shear zone, a number of smaller lozenges are isolated to form compartments (arrow 1 in Fig. 3.10), whereas compartmentalization is not yet complete in other cases (arrows 2 and 3 in Fig. 3.10).

The degree of mylonitic overprint of the lozenge increases with decreasing angles between the bounding step-overs and the host shear zones (compare

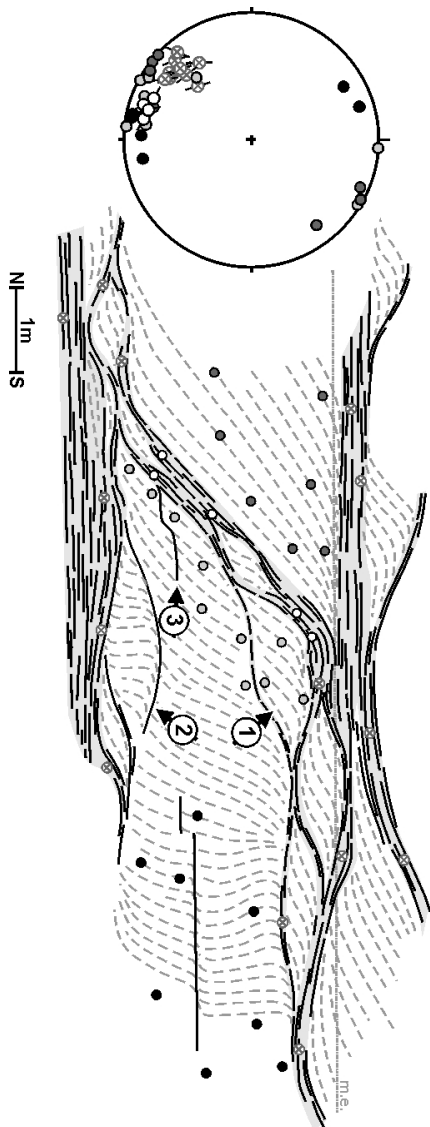


Figure 3.10: A step-over shear zone linking two host shear zones. Small lozenges form along the step-over shear zone. The equal area plot shows the orientations of S₃/L₃ (projection method of Hoepfner, 1955) as well as S₁/2 orientations adjacent to the shear zones. Note the shading of different fabric domains. See text for explanation. Legend as in Fig. 3.9. UTM 31T 521937 east, 4686951 north.

Figs. 3.10 and 3.12). Juvenile step-over shear zones in our investigation area, mostly brittle fractures and thin ultramylonites, are usually subparallel to undeformed D2-fabrics as long as the displacement is relatively small (see equal area plot in Fig. 3.9). Step-overs in highly overprinted rock are usually decimeter-wide mylonitic shear zones making a significantly smaller angle with C3 (Fig. 3.12).

Compartmentalization of lozenges and subsequent incorporation of lozenge rock into the mylonitic D3 shear zones act in concert with the rotation of step-over shear zones to homogenize strain on the scale of the fracture network observed at the onset of interconnection. Figure 3.13 shows an advanced stage of this homogenization process. The volume proportion of D3 mylonite (shaded, black foliation trajectories) roughly equals that of less-deformed host rock (white areas, grey, dashed foliation trajectories). Drags in the lozenges are truncated by fractures (arrow 1 in Fig. 3.13).

The northernmost part of the Cala Serena (Fig. 8 in Carreras, 2001) shows a mature stage of network evolution, where the volume proportion of D3 mylonites is relatively large and deformation is almost homogeneous on a scale of several tens of meters. A single D3 shear zone - almost 50m wide - contains only small-scale lozenges up to 3m in length.

3.5 Discussion and interpretation

3.5.1 Evidence for a strain dependent BVT

Several arguments indicate that fracturing occurred coevally with mylonitization during retrograde deformation at temperatures between 400 and 500°C (Fusseis & Handy, 2006):

1. Most of the observed fractures, irrespective of their occurrence individually or in damage zones, are parallel to mylonitic fabrics of the ductile shear zones (equal area plot in Fig. 3.5a). Ductile beads as well as drags near brittle fractures indicate the same movement sense as obtained from independent kinematic indicators within the ductile shear zones (Figs. 3.3 and 3.4). None of the fractures in these orientations was seen to cross-cut or overprint D3 mylonites, neither on the outcrop nor on the microscopic scales (Fusseis & Handy, 2006). Brittle overprinting of D3 fabrics is restricted to D4 faults that possibly formed during E-W Tertiary extension of the area (e.g. Mauffret et

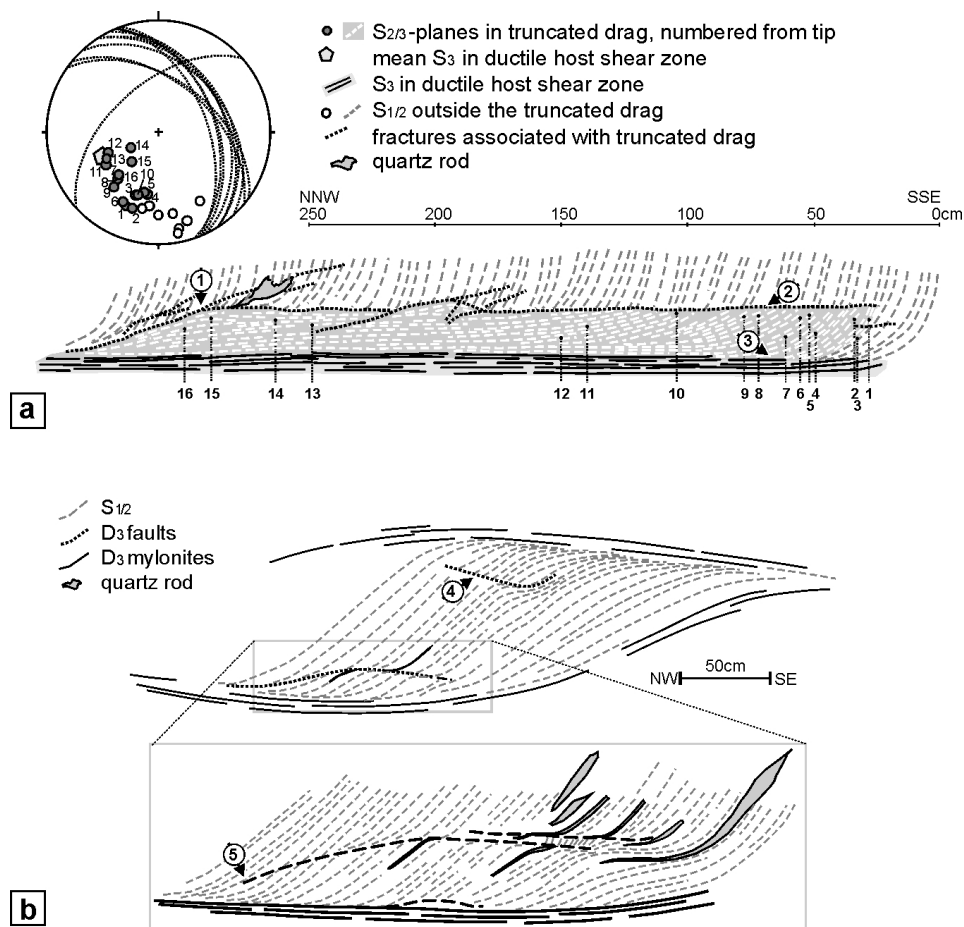


Figure 3.11: Shear zone widening: (a) A shear zone boundary in Cala Prona reveals the 'drag truncation' process. The lower hemisphere, equal area plot shows the foliation orientation within the isolated domain and its rotation into parallelism with the host shear zone at the bottom; UTM 31T 521755 east, 4687572 north. (b) Sketch of a lozenge in the Cala Serena illustrating drag truncation on a smaller scale within a lozenge in a mature mylonitic shear zone. Note the footwall drag truncation at the top of the lozenge (arrow 4). UTM 31T 521585 east, 4687106 north.

al., 2001). Hydrothermal alterations and the kinematics of these D4 faults clearly allows one to distinguish them from D3 fractures.

2. The displacement-distance relationship in Figure 3.6 clearly shows a constant increase in displacement going from the fractures to the mylonite, as shown in Fig 3.5. If fractures had nucleated at the tips of mylonitic shear zones after mylonitization, they would be expected to have developed independent, symmetrical displacement-distance pro-

files (cf. Cowie & Shipton, 1998 and references therein).

3. The process of drag truncation involves both brittle fractures and mylonitic shear zones. Even though we do not know if the drags were fractured during mylonitic shearing or the fractures are reactivated remnants of fractures formed early during D3, synkinematic fractures segment parts of ductile drags. The reoriented fabrics within these segmented, isolated domains experienced a greater degree of mylonitic overprint and thus are enveloped within the broadening shear zones (Fig. 3.11a). Therefore, fracturing is an integral process in the widening of mylonitic shear zones.
4. Microstructural investigations indicate upper-greenschist facies conditions for the formation of centimeter-scaled fractures in tip damage zones of mylonitic shear zones, which are in structural continuity with quartz-rich parts of the rock undergoing increased dynamic recrystallization by bulging and subgrain rotation (Fusseis & Handy, 2006).

3.5.2 A model for the formation, propagation and networking of shear zones at the BVT

Having established that fracturing and viscous mylonitic creep were coeval, we advance the following propagation model for shear zones at the BVT (Fig. 3.14a): Pre-D3 fabric domains are expected to have shown heterogeneous mechanical behaviour during loading. Initial flaws nucleated at pre-existing heterogeneities. These flaws are interpreted as predominantly mode 2 fractures, because they show little to no dilation and are parallel to the later shear zones. Creep in the ductile beads in front of the fault tips is interpreted to have dissipated some of the strain energy stored during loading and lead to localized softening there. However, the rate of stress relaxation in the ductile beads was less than the overall rate of loading, so that the brittle strength of the rock at the fault tip was exceeded and the fracture propagated into its viscously deforming process zone. Such episodic frictional instability leading to faulting during creep has been discussed recently by Handy & Brun (2004).

Brittle fractures are not longer than about 7 to 8 meters in any of the investigated sites and no isolated, mylonitic shear zones were found that are shorter than this length. Therefore, it stands to reason that once a growing

fault system acquired a critical length and displacement, mylonitic shearing replaced episodic fracturing as the dominant deformation mechanism. The transition was controlled by the combined effects of brittle segmentation of the ductile bead at ambient temperatures of $> 400^{\circ}\text{C}$, dynamic recrystallization of quartz and syntectonic recrystallization of biotite, which together softened the host rock in the tip process zone (Fig. 3.5, Fousseis & Handy, 2006). There is no evidence for a major influx of externally derived hydrous fluids. Shear zone evolution documented in Fig. 3.5 indicates that the critical total displacement necessary to soften the host rock sufficiently for a transition from predominantly brittle to viscous deformation was around 120cm along a 140cm wide shear zone.

The sharp cut-offs of normal drags along many drags indicate that the drags formed when fractures propagated through ductile beads (de Margerie & Heim, 1888, Elliott, 1976). The detailed shape, curvature and dimension of beads and consequently of drags were influenced by the deformed lithology as well as by interaction and interconnection with other fractures (Fig. 3.4). The formation of mylonitic shear zone centers during a strain-dependent BVT transformed sharp cut-offs into smooth cut-offs. This modified the drag shape.

We interpret the step-overs to have formed due to strain compatibility requirements that arose from accumulating displacement along the host shear zones, in analogy with the model proposed by Mitra (1979). Rotating step-over shear zones forced the intervening lozenges to deform internally. This effect was strongest at the intersections between step-over and host shear zones, which was where most compartments were observed (Figs. 3.10 and 3.13).

The question why softening shear zones widen by drag truncation is crucial. Fractures that already existed within the damage zone of a mylonitic shear zone would have eased rotation and thus mylonitic overprint of $S1/2$ in these domains. Fractures that truncated existing drag and propagated during shearing (which is supported by field evidence, Fig. 3.11a) indicate a competition between the rate of strain energy dissipation in the shear zone center and the loading rate of the system, similar to the model proposed above for the fault propagation in ductile beads.

The overall driving mechanism for shear zone widening may be a combination of strain energy minimization and maintenance of strain compat-

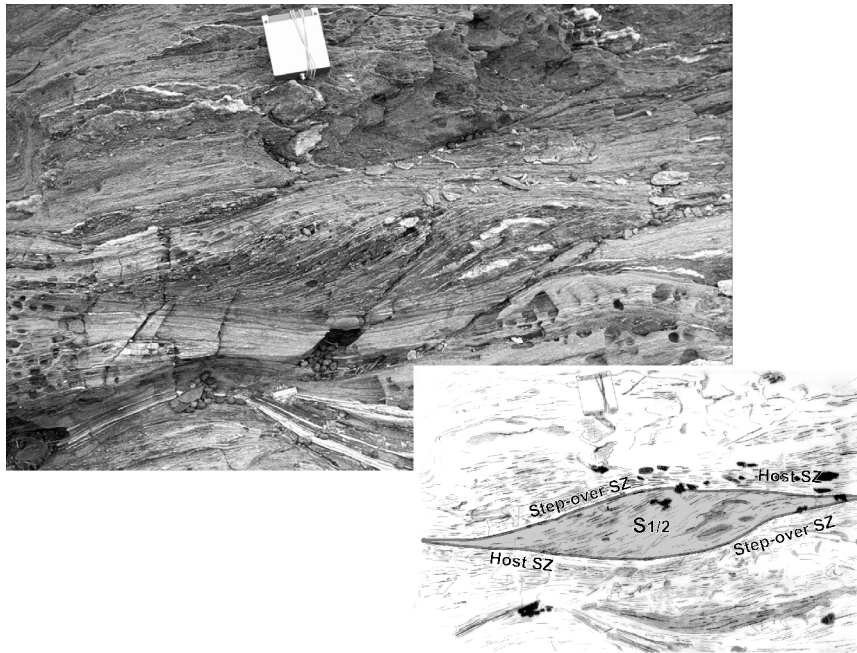


Figure 3.12: Mature lozenge in a highly deformed part of the Cala Serena SZN. Pre-D3 mineral assemblages are preserved in the lozenge interior (notice coarse grainsize), whereas the material in the surrounding host and step-over shear zones experienced a significant D3 mylonitic overprint. Compass for scale, sidelength ~8cm. View towards the east. Location in inset "12" of Fig. 3.1, UTM 31T 521687 east, 4686903 north.

ibility. If the shear zones can be compared to slip systems in crystals (as proposed by Mitra, 1979), then applying Von Mises' criterion to our (plane strain) case would support the idea that the two shear zone types (host and step-over shear zones) are insufficient in number to accommodate the bulk shearing compatibly. A third independent shear zone orientation does not form, possibly because shear zone widening by rotation of S1/2 into the shearing plane allows bulk deformation to become heterogeneous on a larger length scale, thereby expending less bulk strain energy per unit volume and time and maximizing the rate of strain energy dissipation per unit volume of deforming rock. As a consequence, the length scale of heterogeneous strain increases with displacement.

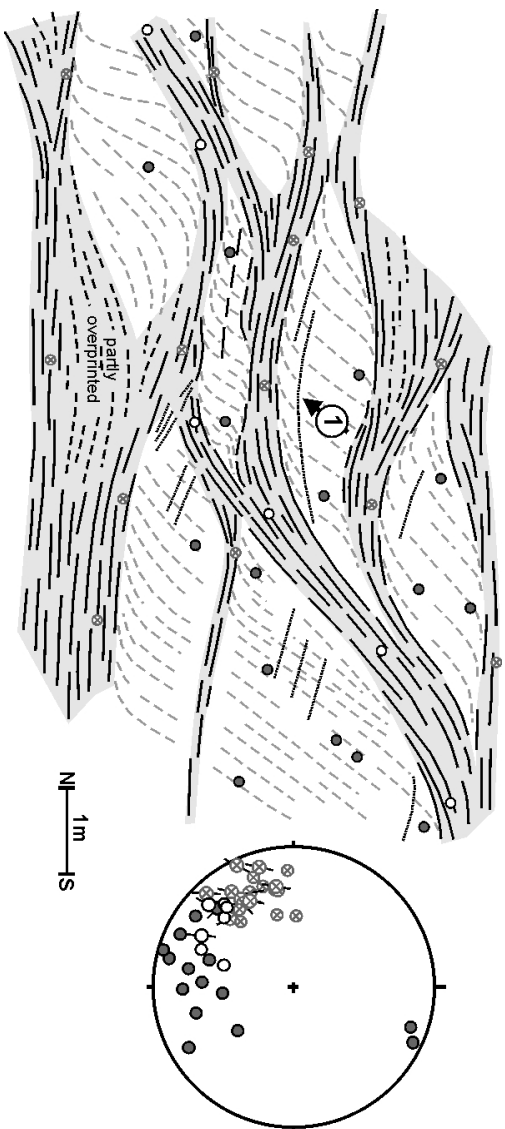


Figure 3.13: Mature pattern of interconnected shear zones. The remaining D2 domains are progressively incorporated into the D3 shear zones. Note fractures in dragged margins of the lozenges (arrow 1). The lower hemisphere, equal area plot shows the orientations of S3/L3 (projection method of Hoepfner, 1955) as well as S2 orientations adjacent to the shear zones. Note the shading of different fabric domains. Legend as in Fig. 3.9. UTM 31T 521948 east, 4686935 north.

3.5.3 Bulk kinematics and scales of strain localization

Carreras (2001) invoked analogue models of folded anisotropies (Cobbold et al., 1971, Cosgrove, 1976, 1989; Williams & Price, 1990) to propose buckling instabilities as the prime nucleation mechanism for the shear zones in the "Northern Shear Belt" (cf. Fig. 18 in Carreras, 2001). Carreras argued that the instantaneous shortening direction for D3 (ISA^-) was oriented approximately N-S. Depending on the orientation of S1/2 with respect to this ISA^- , different shear zone geometries resulted from the rotation and shearing of the limbs of folds that formed due to buckling of S1/2. In areas like ours where the initial angle between the inferred ISA^- and the ENE-WSW trending S1/2 was high ($\sim 80^\circ$), Carreras (2001) proposed that a single set of dextral shear zones initiated close to the direction of maximum instantaneous stretch and rotated into parallelism with the bulk shearing plane, which trends approximately NW-SE. In areas where the angle between S1/2 and the ISA^- was small, a conjugate set of shear zones evolved, with synthetic shear zones nucleating close to the bulk shearing plane and antithetic shear zones close to the plane of maximum instantaneous shear strain, nearly normal to the shearing plane (Fig. 18 in Carreras, 2001).

The buckling model of shear zone formation (Carreras, 2001) explains the orientation of the host shear zones in the investigated area, but it is incompatible with the E-W trending step-over shear zones and does not explain the close association of fractures and mylonitic shear zones. Furthermore, we note that the E-W trending step-overs and host shear zones did not nucleate coevally. Rather, the step-overs are usually younger, as they branch from the better-developed, host shear zones which accommodated more deformation.

The step-over shear zones nucleated at angles of about 60° - 80° to the bulk shearing plane, C3, suggesting that S1/2 at high initial angles to C3 guided the propagation of juvenile step-overs, as described above. Shear zones with this orientation are expected to have accommodated sinistral shear in the bulk dextral regime. With increasing bulk deformation, the step-overs rotated across ISA^+ towards C3. Upon crossing this axis, they accommodated pure shear before their shear sense changed to dextral, as observed in experiments on networked shear zones formed in noncoaxial shear (Herwegh & Handy, 1996, 1998) and proposed by Carreras (2001, see his Fig. 18). This may explain the ambiguous shear sense indicators in most

of the step-over shear zones.

The orientational distribution pattern of networked shear zones in Figure 3.8 reflects both the kinematic vorticity and the shape of the finite strain ellipsoid during D3 (Gapais et al., 1987). As pointed out above, the slight asymmetry of the maxima for the poles to S3 reflects the orientations of the host- and step-over shear zones with respect to the shearing plane. The broad single maximum of the poles to S3 (Fig. 3.8a) indicates that the lozenges are oblate, its asymmetry indicates non-coaxial shearing. The single maximum in the L3 equal area plot points towards a stretching direction typical of near plane-strain deformation (Fig. 3.8b). Considered together, the orientational distribution pattern is diagnostic of strongly non-coaxial nearly plane-strain dextral shearing during D3 (Gapais et al., 1987, Handy et al. in press). We note that this justifies our generalizations about shearing made from the study of strain in two dimensions.

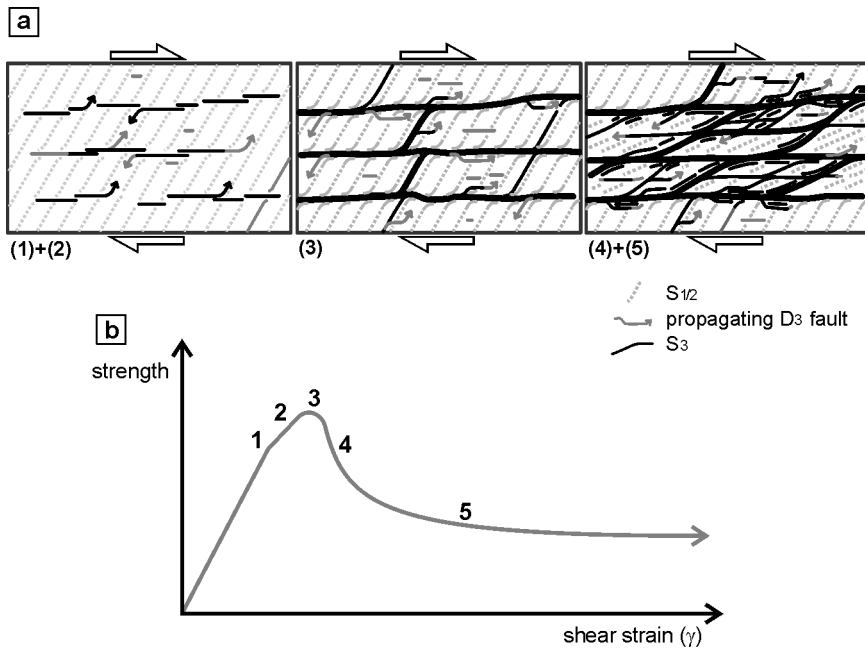


Figure 3.14: Model for the structural and mechanical evolution of shear zone networks on a 10^2 to 10^3 meter-scale: (a) Fracture propagation and coalescence of shear zones corresponding to the mechanical evolution in (b); (b) Inferred evolution of rock strength with progressive shear strain. See text for explanations.

3.5.4 Implications for crustal strength at the BVT

The strength of the crust affected by shear zone networking at the BVT is expected to have decreased significantly during strain localization (Fig. 3.14b). The nucleation of shear fractures in the host rock is inferred to have coincided with yielding (pt. 1 in Fig. 3.14b). Continued loading promoted fracture lengthening, incipient interconnection and the accumulation of displacement. Mylonite formed after the fractures reach a critical length and displacement (respectively, 7 - 8 meters and 80 - 120 cm in our examples). Grain-size reduction involving dynamic recrystallization and the nucleation and growth of weaker phases (mica) weakened the shear zone, focussing deformation along its central, high-displacement segment and reducing the rate at which strain energy accrued in the deforming system (pt. 2 in Fig. 3.14b). Because viscous creep is rate-strengthening (e.g. Scholz, 1988), mylonitization prevented run-away weakening and dampened stress pulses associated with fracturing at the shear zone tips.

The peak strength of the deforming system is predicted to have coincided with the maximum number of isolated fractures and ductile shear zones per volume of deforming rock, i.e., the state of the system just prior to full networking (pt. 3 in Fig. 3.14b). This is when the aspect ratio of isolated shear zones and the maximum number of propagating tips reached a maximum. We note that the onset of localization prior to the attainment of peak strength predicted for the fossil BVT at the Cap de Creus is consistent with the behavior of some dilatant materials, including viscoplastic materials whose deformation involves limited dilatancy (Hobbs et al., 1990).

The coalescence of individual shear zones lead to the formation of a three-dimensional network, as described in the previous sections. Networking is expected to have induced a rapid drop in strength of the deforming system (curve from pts. 3 to 4 in Fig. 3.14b) once the networked mylonitic shear zones formed an interconnected weak layer subparallel to the bulk shearing plane. A strength drop due to networking of weak phases has been proposed based on theoretical considerations and experiments on two-phase aggregates (e.g. Handy, 1990, 1994 and references therein). A possible reason for the networking could be the necessity to maintain strain compatibility within the deforming system, i.e. the entire rock including the shear zones and the existing $S1/2$ (Mitra, 1978). Our observations indicate that juvenile shear zone networks are about 50-100m wide and maintained this overall width

with continued deformation. Within this limit, the networked shear zones widened, promoting continued overall weakening (curve from pts. 4 to 5 in Fig. 3.14b) as the volume proportion of weak, mylonitic rocks increased in the deforming system (Handy, 1994). A factor controlling shear zone widening may be the rotation of the step-over shear zones, which required overprinting of the lozenge interiors.

The rate of weakening is expected to have decreased until some stable volume proportion of sheared rock was reached, or when all un- or less-deformed host rock in the lozenges was incorporated in D3 shear zones. At this stage, strain homogenized on the length scales of fracturing and networking, but became heterogeneous on all larger length scales. Therefore, rock strength must be considered to be strongly scale-dependent.

3.6 Conclusions

Brittle faults were precursors to mylonitic shear zones in the shear zone networks at the fossil BVT exposed at the Cap de Creus, NE Spain. Fracturing was accompanied by viscous mylonitic deformation of the host rock in ductile damage zones surrounding the fractures. Brittle segmentation and the mylonitic overprint of host rock in these damage zones lead to a strain-dependent transition from brittle faulting to mylonitic shearing. This is inferred to have involved strain-softening. Once ductile shear zones formed, drag-truncation, involving brittle fracturing, allowed shear zones to continue widening on scales from decimeters to several meters while they experienced strain softening.

Interconnection of shear zones and fractures was influenced by the existing foliation orientated at high angles to the shearing plane. This foliation guided the propagating fracture tips. Initial shear zone networks are defined by lozenges some 10 to 20m long and 5 to 10m wide. The lozenges between the networked shear zones were progressively compartmentalized by drag truncation and incorporated into the shearing volume of rock. Finally, strain became homogeneous at the initial length scale of networking.

The strength evolution of the crust at the BVT is governed by the transition from predominantly brittle fracturing to mylonitic shearing, the interconnection of individual shear zones to form networks and the homogenization of deformation on the scale of those networks. Strain localization

in shear zone networks can be expected to weaken the crust on the scale of these networks by up to 20% (Handy, 1994).

3.7 Acknowledgements

We thank Jordi Carreras and Elena Druguet for their generous support in organizing field campaigns, aerial photographs and permits from the national park authorities. They also kindly supplied several unpublished maps and data, and provided fruitful discussions and comments on our work. Victoria Riera and the national park authorities are thanked for their uncomplicated support. Many thanks also to Ian Alsop and Jonathan Imber for their helpful and vigilant reviews, as well as to an anonymous reviewer for some critical points. We especially want to thank Bob Holdsworth for his mindful editing of the manuscript. Finally, we thank Roland Christmann and several students from the Freie Universität Berlin who contributed to this work with their help in the field and at home. Our work was supported by DFG grant Ha 2403/6 and by the Freie Universität Berlin in the form of a post-graduate studentship.

